The redox series [Ru(bpy)$_2$(L)]^n, n = +3, +2, +1, 0, with L = bipyridine, "click" derived pyridyl-triazole or bis-triazole: a combined structural, electrochemical, spectroelectrochemical and DFT investigation†

Stephan Hohloch,[a] David Schweinfurth,[a] Michael G. Sommer,[a] Fritz Weisser,[a] Naina Deibel,[b] Fabian Ehret[b] and Biprajit Sarkar*[a]

The compounds [Ru(bpy)$_2$(L^1)](ClO$_4$)$_2$ (**1**(ClO$_4$)$_2$), [Ru(bpy)$_2$(L^2)](ClO$_4$)$_2$ (**2**(ClO$_4$)$_2$), [Ru(bpy)$_2$(L^3)](ClO$_4$)$_2$ (**3**(ClO$_4$)$_2$), [Ru(bpy)$_2$(L^4)](ClO$_4$)$_2$ (**4**(ClO$_4$)$_2$), [Ru(bpy)$_2$(L^5)](ClO$_4$)$_2$ (**5**(ClO$_4$)$_2$), and [Ru(bpy)$_2$(L^6)](ClO$_4$)$_2$ **6**(ClO$_4$)$_2$ (bpy = 2,2'-bipyridine, L^1 = 1-(4-isopropyl-phenyl)-4-(2-pyridyl)-1,2,3-triazole, L^2 = 1-(4-butoxy-phenyl)-4-(2-pyridyl)-1,2,3-triazole, L^3 = 1-(2-trifluoromethyl-phenyl)-4-(2-pyridyl)-1,2,3-triazole, L^4 = 4,4'-bis-{1-(2,6-diisopropyl-phenyl)}-1,2,3-triazole, L^5 = 4,4'-bis-{(1-phenyl)}-1,2,3-triazole, L^6 = 4,4'-bis-{1-(2-trifluoromethyl-phenyl)}-1,2,3-triazole) were synthesized from [Ru(bpy)$_2$(EtOH)$_2$](ClO$_4$)$_2$ and the corresponding "click"-derived pyridyl-triazole or bis-triazole ligands, and characterized by ^{1}H-NMR spectroscopy, elemental analysis, mass spectrometry and X-ray crystallography. Structural analysis showed a distorted octahedral coordination environment about the Ru(II) centers, and shorter Ru−N-(triazole) bond distances compared to Ru−N(pyridine) distances in complexes of mixed-donor ligands. All the complexes were subjected to cyclic voltammetric studies, and the results were compared to the well-known [Ru(bpy)$_3$]$^{2+}$ compound. The oxidation and reduction potentials were found to be largely uninfluenced by ligand changes, with all the investigated complexes showing their oxidation and reduction steps at rather similar potentials. A combined UV-vis-NIR and EPR spectroelectrochemical investigation, together with DFT calculations, was used to determine the site of electron transfer in these complexes. These results provided insights into their electronic structures in the various investigated redox states, showed subtle differences in the spectroscopic signatures of these complexes despite their similar electrochemical properties, and provided clues to the unperturbed redox potentials in these complexes with respect to ligand substitutions. The reduced forms of the complexes display structured absorption bands in the NIR region. Additionally, we also present new synthetic routes for the ligands presented here using Cu-abnormal carbene catalysts.

Introduction

Substituted 1,2,3-triazole ligands synthesized *via* the Cu(I) catalyzed "click" reaction between alkynes and azides[1] have found a prominent place in the coordination chemists toolbox in recent years.[2] Metal complexes of these ligands have been investigated for various research objectives such as electron transfer properties,[3a–h] photochemistry,[4] supramolecular chemistry,[5] magnetism,[6] catalysis[7] and anti-tumor agents.[8] We have been interested in applying metal complexes of substituted 1,2,3-triazole ligands in various fields of chemistry. Thus, we have investigated Pd(II) and Pt(II) complexes with bidentate pyridyl-triazole ligands for their electron transfer properties,[9] Co(II) and Ni(II) complexes with tripodal triazole ligands for their magnetic properties,[10] Fe(II) and Co(II) complexes of tripodal triazole ligands and Ni(II) complexes of pyridyl-triazole ligands as pre-catalysts for ethylene poly- and oligomerisation,[11] Cu(I) complexes of abnormal carbenes derived from 1,2,3-triazoles as catalysts for the azide–alkyne "click" cycloaddition reaction,[12] and Pd(II) complexes of abnormal carbenes for the Suzuki–Miyaura cross-coupling reactions.[13]

[a]Institut für Chemie und Biochemie, Anorganische Chemie, Freie Universität Berlin, Fabeckstraße 34-36, D-14195 Berlin, Germany. E-mail: biprajit.sarkar@fu-berlin.de
[b]Institut für Anorganische Chemie, Universität Stuttgart, Pfaffenwaldring 55, D-70550 Stuttgart, Germany

Since investigating the electronic and geometric structures of metal complexes is an all important goal in coordination chemistry,[14] and since our group has been using a combined electrochemical, spectroelectrochemical and theoretical approach to address the electronic structures of various metal complexes,[15] we were interested in investigating a series of metal complexes with a redox-active metal center where the electronic properties of the "click" derived ligands would be varied by choosing different azides for ligand synthesis. Ruthenium complexes with "click" derived triazole ligands have been investigated in this context. However, most of these studies are restricted to cyclic voltammetry and DFT calculations.[3f–h] To the best of our knowledge, the only studies that have applied a combined approach of various techniques including spectroelectrochemistry for addressing issues related to the electronic structures of such complexes are the ones where diruthenium complexes with "click" derived ligands have been investigated for their mixed-valent properties.[3d] The electronic and electrochemical properties of the ruthenium complexes of 1,2,4-triazoles have been previously investigated by Vos et al.[3i,j]

In the following, we present the synthesis and characterization of the complexes $[Ru(bpy)_2(L^1)](ClO_4)_2$ ($1(ClO_4)_2$), $[Ru(bpy)_2(L^2)](ClO_4)_2$ ($2(ClO_4)_2$), $[Ru(bpy)_2(L^3)](ClO_4)_2$ ($3(ClO_4)_2$), $[Ru(bpy)_2(L^4)](ClO_4)_2$ ($4(ClO_4)_2$), $[Ru(bpy)_2(L^5)]$-$(ClO_4)_2$ ($5(ClO_4)_2$), and $[Ru(bpy)_2(L^6)](ClO_4)_2$ $6(ClO_4)_2$ (bpy = 2,2′-bipyridine, L^1 = 1-(4-isopropyl-phenyl)-4-(2-pyridyl)-1,2,3-triazole, L^2 = 1-(4-butoxy-phenyl)-4-(2-pyridyl)-1,2,3-triazole, L^3 = 1-(2-trifluoromethyl-phenyl)-4-(2-pyridyl)-1,2,3-triazole, L^4 = 4,4′-bis-{1-(2,6-diisopropyl-phenyl)}-1,2,3-triazole, L^5 = 4,4′-bis-{(1-phenyl)}-1,2,3-triazole, L^6 = 4,4′-bis-{1-(2-trifluoromethyl-phenyl)}-1,2,3-triazole). The ligands L have been varied from pyridyl-triazole to bis-triazoles with the electronic properties of the substituents on the triazole rings being different in each case. Results obtained from ^{1}H-NMR spectroscopy, elemental analysis, single crystal X-ray crystallography, cyclic voltammetry, UV-vis-NIR and EPR spectroelectrochemistry and DFT calculations are presented. The compounds are compared with the parent compound $[Ru(bpy)_3]^{2+}$. The data obtained from this combined approach are used to understand the properties of these complexes and to rationalize the observed trends.

Results and discussion

Synthesis and crystal structure

The pyridyl-triazole ligands L^1–L^3 have been reported by us previously.[9,11b] In this work, we used a new synthetic route developed in our laboratory for synthesizing the ligands L^1 and L^2.[12] The new route takes advantage of the highly robust and oxidation resistant Cu(I)-abnormal carbene catalysts for catalyzing the "click" reaction. This procedure delivered L^1 and L^2 in superior yields to those reported by us previously (see the Experimental section). The bis-triazole ligands L^4–L^6 were prepared by modifications of literature procedures.[3c,16] To the best of our knowledge, the ligand L^6 has not been reported
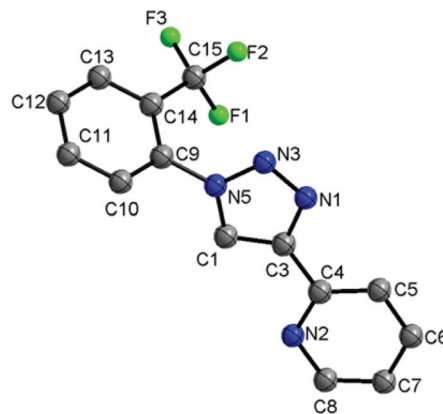
Fig. 1 ORTEP plot of L^3. Ellipsoids are drawn at 50% probability. Hydrogen atoms and solvent molecules have been omitted for clarity.

elsewhere. Single crystals of L^3 were obtained by slow evaporation of a diethylether solution at room temperature. L^3 crystallizes in the tetragonal $I4_1/a$ space group with 0.31 molecule of strongly disordered diethylether (Table S1†). The central N1=N3 bond of the triazole rings in L^3 and $L^{4\,7g}$ are 1.303(2) and 1.305(2) Å, respectively (Table 2, Fig. 1), and these distances are typical of a N=N double bond. That bond in both the ligands is flanked by N1–C3 and N3–N5 bonds which are longer than N1=N3 (Table 2). Thus, the best localized description of the bonding situation in these triazole rings is that of a central N=N double bond flanked by N–C and N–N single bonds. Similar observations have been made by us and others previously.[9,17]

The pyridyl-N atom is *anti* to the triazole N atoms in L^3. The pyridyl and the triazole rings are almost coplanar with a dihedral angle of only 2.87(7)°. In contrast, the 2-(trifluoromethyl)-phenyl is largely twisted with respect to the triazole ring with a dihedral angle of 65.29(7)° (Fig. 1). The two triazole rings in L^4 are *anti* to each other. The deviation from planarity of those rings is minimal as seen from a dihedral angle of 9.05(7)°. The two 2,6-(diisopropyl)-phenyl substituents are almost perpendicular to the triazole rings with dihedral angles of 89.90(7)° and 88.45(7)°.[7g]

For the synthesis of the complexes, $Ru(bpy)_2Cl_2$ was first activated with $AgClO_4$ to generate $[Ru(bpy)_2(EtOH)_2](ClO_4)_2$ through extraction of the chloride ions and precipitation of AgCl. The thus *in situ* generated $[Ru(bpy)_2(EtOH)_2](ClO_4)_2$ was reacted with the ligands L^1–L^6 under reflux in ethanol to generate the complexes $1(ClO_4)_2$–$6(ClO_4)_2$ respectively (Fig. 2). Chromatography on alumina and subsequent precipitation with $NaClO_4$ delivered analytical pure complexes (see the Experimental section). The purity of the complexes was demonstrated by ^{1}H NMR spectroscopy, elemental analysis, and mass spectrometry.

Crystals of $3(ClO_4)_2$, $4(ClO_4)_2$ and $6(ClO_4)_2 \cdot CH_2Cl_2$ for single crystal X-ray diffraction studies were obtained by slow diffusion of *n*-hexane into dichloromethane. $3(ClO_4)_2$ and $6(ClO_4)_2 \cdot CH_2Cl_2$ crystallize in the triclinic $P\bar{1}$ space group, and $4(ClO_4)_2$ in the monoclinic $P2_1/n$ space group (Table 1). The bond lengths and bond angles within these three complexes
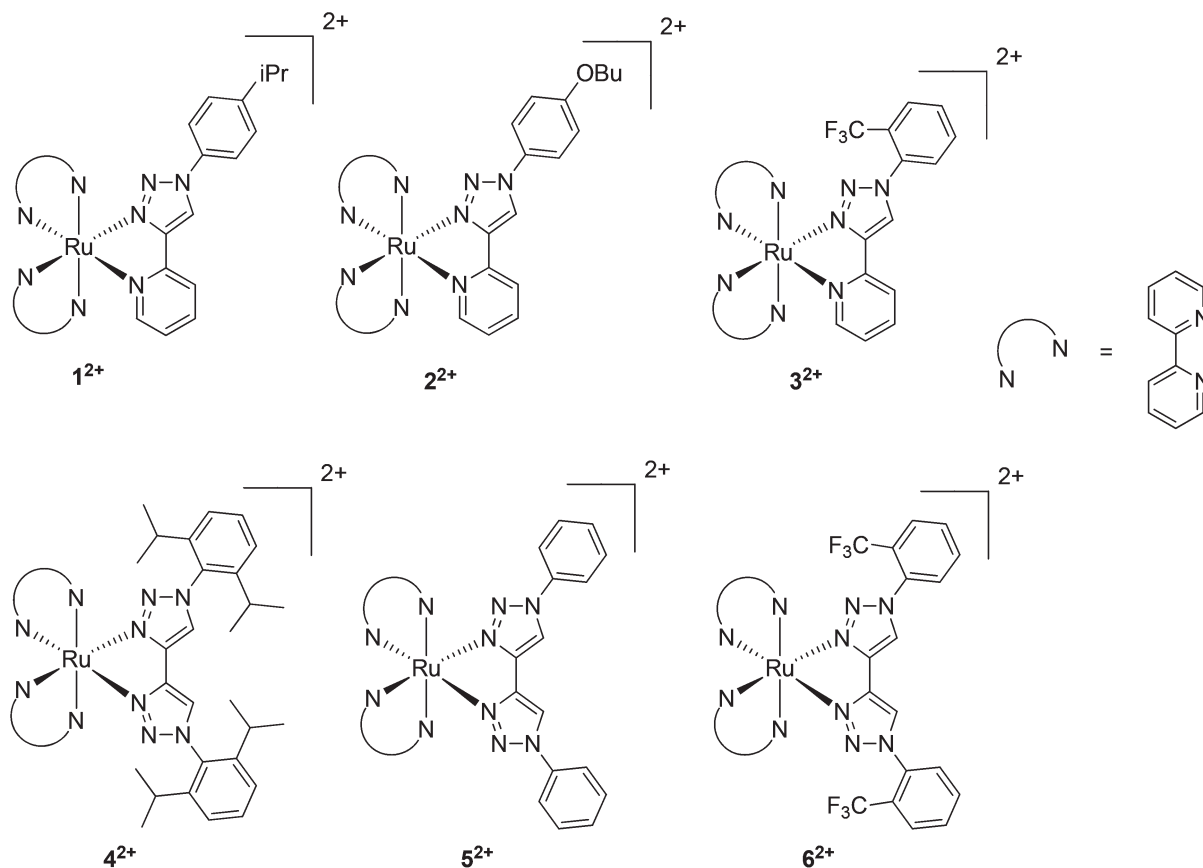
Fig. 2 Complexes synthesized for the present study.

thus present us with the opportunity to compare the complexes with pyridyl-triazole ligands with those of bis-triazoles. In all the three complexes, the ruthenium center is co-ordinated in a distorted octahedral environment, the distortion being caused by the chelating nature of the ligands, as well as the presence of different kinds of donor atoms. The donor atoms in all cases are the four pyridine-N atoms from the two bpy ligands, and the pyridine and/or triazole N donors from the third chelating ligand (Fig. 3–5, Tables 3 and 4).

The Ru–N bond distances to the four N atoms of the two bpy rings are all in a similar range for all three complexes (Table 3), and match well with distances for similar complexes reported in the literature.[18] Comparison of the Ru–N(triazole) distances in the three complexes shows some similarities and

Table 1 Crystallographic details of complexes

	3 (ClO$_4$)$_2$	**4** (ClO$_4$)$_2$	**6** (ClO$_4$)$_2$·CH$_2$Cl$_2$
Chemical formula	C$_{34}$H$_{25}$N$_8$F$_3$Ru Cl$_2$O$_8$	C$_{48}$H$_{52}$N$_{10}$Ru Cl$_2$O$_8$	C$_{38}$H$_{26}$N$_{10}$F$_6$Ru Cl$_2$O$_8$ CH$_2$Cl$_2$
M_r	902.59	1068.97	1121.58
Crystal system, space group	Triclinic, $P\bar{1}$	Monoclinic, $P2(1)/n$	Triclinic, $P\bar{1}$
a, b, c (Å)	10.6547(12), 11.6352(12), 14.5178(16)	18.5069(12), 15.2755(11), 19.3531(13)	11.199(2), 12.433(2), 16.087(3)
α, β, γ (°)	89.532(5), 77.126(5), 87.806(4)	90, 116.969(4), 90	89.218(4), 87.674(4), 88.700(4)
V (Å^3)	1753.2(3)	4876.2(6)	2237.2(7)
Z	2	4	2
Density (g cm^{-3})	1.710	1.456	1.665
$F(000)$	908	2208	1124
Radiation type	Mo K$_\alpha$	Cu K$_\alpha$	Mo K$_\alpha$
μ (mm^{-1})	0.681	4.142	0.678
Crystal size	0.27 × 0.17 × 0.07	0.20 × 0.15 × 0.02	0.8 × 0.25 × 0.08
Meas. Refl.	24 195	28 019	31 477
Indep. Refl.	7226	8249	10 966
Obsvd. [$I > 2\sigma(I)$] refl.	5206	5749	9419
R_{int}	0.0565	0.0692	0.0200
R [$F^2 > 2\sigma(F^2)$], w$R(F^2)$, S	0.0406, 0.0764, 1.005	0.0464, 0.1228, 1.013	0.0821, 0.2396, 1.045
$\Delta\rho_{max}$, $\Delta\rho_{min}$ (e Å^{-3})	0.523, −0.549	1.152, −0.526	4.828, −2.990

Table 2 Selected bond lengths of the ligands in Å

	$L^3 \cdot 0.31\ Et_2O$	$L^{4,7g}$
C1–C3	1.367(3)	1.366(2)
N1–N3	1.303(2)	1.305(2)
N1–C3	1.361(3)	1.362(2)
N3–N5	1.353(2)	1.352(2)
N5–C1	1.344(2)	1.350(2)
N2–C4	1.335(3)	1.364(2)
C3–C4	1.468(3)	1.454(2)
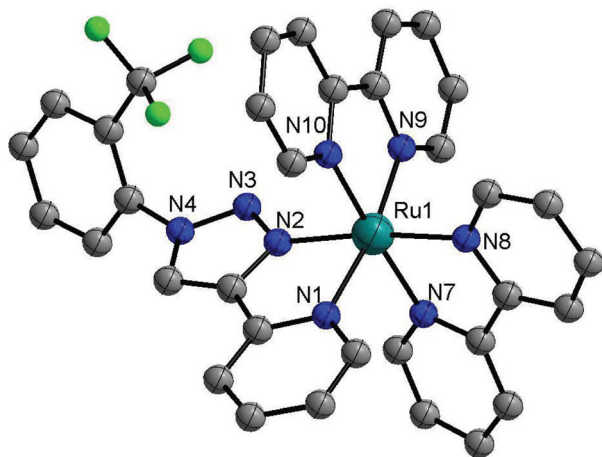
Fig. 3 ORTEP plot of **3**(ClO₄)₂. Ellipsoids are drawn at 50% probability. Hydrogen atoms and counter ions have been omitted for clarity.
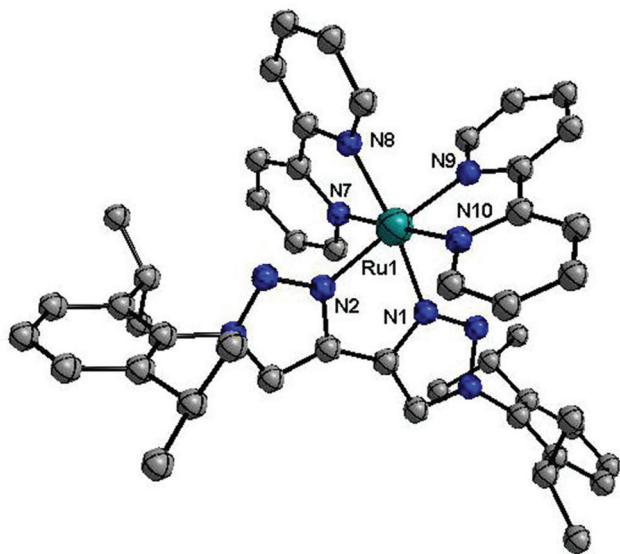
Fig. 4 ORTEP plot of **4**(ClO₄)₂. Ellipsoids are drawn at 50% probability. Hydrogen atoms and counter ions have been omitted for clarity.

Fig. 5 ORTEP plot of **6**(ClO₄)₂·CH₂Cl₂. Ellipsoids are drawn at 50% probability. Hydrogen atoms, solvent molecule and counter ions have been omitted for clarity.

Table 3 Selected bond lengths in the complexes in Å

	3 (ClO₄)₂	**4** (ClO₄)₂	**6** (ClO₄)₂·CH₂Cl₂
N1–Ru1	2.090(3)	2.065(3)	2.054(4)
N2–Ru1	2.026(3)	2.052(3)	2.060(4)
N7–Ru1	2.055(3)	2.070(3)	2.057(4)
N8–Ru1	2.049(1)	2.059(3)	2.048(4)
N9–Ru1	2.051(3)	2.062(3)	2.049(4)
N10–Ru1	2.044(3)	2.068(4)	2.062(4)

Table 4 Selected bond angles in the complexes in °

	3 (ClO₄)₂	**4** (ClO₄)₂	**6** (ClO₄)₂·CH₂Cl₂
N1–Ru–N2	78.3(1)	76.9(1)	77.4(2)
N2–Ru–N10	85.4(1)	82.9(1)	89.9(2)
N10–Ru–N9	78.8(1)	79.0(1)	78.9(2)
N9–Ru–N8	94.0(1)	86.7(1)	90.3(2)
N8–Ru–N7	78.7(1)	78.4(1)	79.2(2)
N2–Ru–N9	94.4(1)	96.5(1)	95.9(1)
N2–Ru–N7	98.3(1)	98.7(1)	95.8(2)
N9–Ru–N7	101.7(1)	100.7(1)	94.9(2)
N8–Ru–N1	94.4(1)	100.1(1)	96.5(2)
N10–Ru–N1	95.4(1)	95.3(1)	99.5(2)
N7–Ru–N1	84.7(1)	85.1(1)	87.2(2)
N8–Ru–N10	97.5(1)	100.0(1)	95.8(2)
N1–Ru–N9	170.3(1)	171.9(1)	173.1(2)
N2–Ru–N8	172.4(2)	176.1(1)	172.3(2)
N10–Ru–N7	176.2(2)	178.4(1)	172.1(2)

differences. Thus, in **3**(ClO₄)₂, which contains the mixed donor pyridyl-triazole ligand, the Ru1–N2 distance of 2.026(3) Å to the triazole N donor is the shortest metal–ligand distance in that complex (Table 3). This observation matches earlier reports on metal complexes with mixed donor ligands such as L³.[9] On the

other hand, for **4**(ClO₄)₂ and **6**(ClO₄)₂ that contain bis-triazoles as the third ligand, all the Ru–N distances are almost identical (Table 3). Thus, the shorter Ru–N(triazole) distance in **3**(ClO₄)₂ is probably due to steric and/or packing effects in the crystal.

The bonding situation within the triazole rings in the complexes remains the same as what has been discussed for the free ligands above. Thus, in each case inside the triazole ring we find a central N=N double bond that is flanked by an N–C and an N–N single bond.[9,17] The 2-(trifluoromethyl)-phenyl

ring in $3(ClO_4)_2$ is twisted with respect to the triazole ring with a dihedral angle of 64.6(1)°. For $4(ClO_4)_2$ and $6(ClO_4)_2$, the substituents on the triazole rings are also out of plane as compared to the triazole rings with dihedral angles of 77.4(2)° and 72.1(2)° for $4(ClO_4)_2$ and 83.9(2)° and 86.2(2)° for $6(ClO_4)_2$.

Cyclic voltammetry

The redox properties of the complexes were investigated in both CH_2Cl_2–0.1 M Bu_4NPF_6 and CH_3CN–0.1 M Bu_4NPF_6, and these results were compared to those of the parent complex $[Ru(bpy)_3]^{2+}$. The complexes 1^{2+}–6^{2+} display a reversible one-electron oxidation step in both CH_2Cl_2 and CH_3CN. The shape, position and reversibility of this peak seem to be the same irrespective of the complex measured and the solvent used (Fig. 6, 7, S1† and Table 5). The oxidation potentials of these complexes fall in the same range as that of the parent complex $[Ru(bpy)_3]^{2+}$.[18] Thus, neither the substitution of one or more of the pyridine rings in bpy nor the presence of additional substituents in the triazole rings seems to have any influence on the oxidation potentials of the investigated
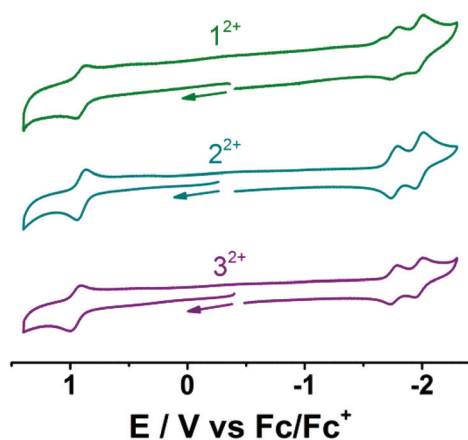
Fig. 6 Cyclic voltammogram of 1^{2+}–3^{2+} in CH_3CN/0.1 M Bu_4NPF_6 at 295 K. Ferrocene/ferrocenium was used as an internal standard.
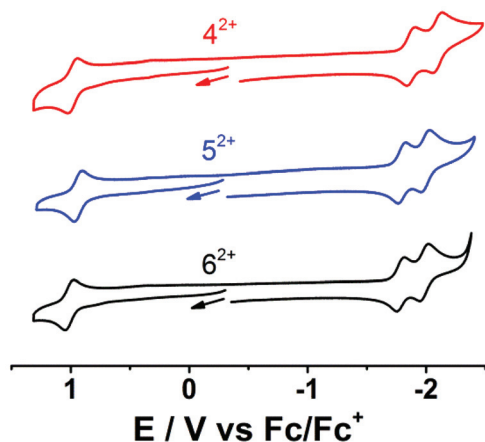
Fig. 7 Cyclic voltammogram of complexes 4^{2+}–6^{2+} in CH_3CN/0.1 M Bu_4NPF_6 at 295 K. Ferrocene/ferrocenium was used as an internal standard.

Table 5 Electrochemical potentials from cyclic voltammetry[a]

	$E_{1/2}^{ox1}$	$E_{1/2}^{red1}$	$E_{1/2}^{red2}$	$E_{1/2}^{red3}$
1^{2+}	0.91	−1.77	−1.97	n.o.
2^{2+}	0.90	−1.77	−1.97	n.o.
3^{2+}	0.95	−1.76	−1.97	n.o.
4^{2+}	0.99	−1.78	−2.00	n.o.
5^{2+}	0.93	−1.79	−2.00	n.o.
6^{2+}	1.01	−1.79	−1.99	n.o.
$[Ru(bpy)_3]^{2+,b}$	0.85	−1.76	−1.92	−2.16

[a] From measurements in CH_3CN–0.1 M Bu_4NPF_6 at 295 K. [b] From ref. 18. n.o. = not observed.

complexes. However, the slightly higher oxidation potential for 4^{2+} and 6^{2+} seems to correlate with the higher dihedral angles between the phenyl substituents and the triazole rings in that molecule as compared to the other cases (see the discussion on the crystal structure above). The oxidation step seems to be totally localized on the ruthenium center (see DFT calculations section), and remains insulated to ligand substitution.

The complex $[Ru(bpy)_3]^{2+}$ displays three one-electron reduction steps in CH_3CN.[18] For complexes 1^{2+}–6^{2+}, only two reduction processes are observed within the CH_3CN solvent window (Fig. 6, 7 and Table 5). Just like the oxidation step, the reduction potentials for both the steps for all the investigated complexes are in the same range, and are comparable to the first two reduction processes of $[Ru(bpy)_3]^{2+}$. These results are already an indication of the first two reduction steps in 1^{2+}–6^{2+} being similar to those of $[Ru(bpy)_3]^{2+}$. As was seen for the oxidation step, ligand substitution does not seem to have an influence on the two observed reduction steps of these complexes either. The third reduction observed in CH_3CN for $[Ru(bpy)_3]^{2+}$ is missing for 1^{2+}–6^{2+} in the same solvent, and this seems to be an effect of substituting one bpy in $[Ru(bpy)_3]^{2+}$ with the ligands L^1–L^6 in the complexes 1^{2+}–6^{2+} respectively. The redox potentials of the complexes reported here are comparable to the analogous complexes of $[Ru(bpy)_2]^{2+}$ with substituted 1,2,4-triazoles. Redox potentials reported by Vos *et al.* against SCE,[3j] if converted against the Fc/Fc⁺ standard, fit well with the redox potentials of the complexes reported here with substituted 1,2,3-triazoles.

Surprisingly, changing the solvent from CH_3CN to CH_2Cl_2 has a large influence on the reversibility, as well as the appearance of the reduction steps for the complexes 1^{2+}–6^{2+} (Fig. S1†). Whereas for 4^{2+} and 5^{2+} the reduction processes in CH_2Cl_2 are similar to that in CH_3CN, the second reduction step in CH_2Cl_2 is irreversible for 1^{2+}–3^{2+}, and it does not show up within the CH_2Cl_2 solvent window for 6^{2+}. For comparison, only two reduction steps are observed for $[Ru(bpy)_3]^{2+}$ in CH_2Cl_2. The reason for the non-observance of certain reduction processes at higher negative potentials in CH_2Cl_2 is related to the smaller potential window of that solvent as compared to CH_3CN.[19] However, even in cases where the same number of reduction processes are observed in both solvents, the reversibility of the reduction steps seems to be better in CH_3CN as compared to CH_2Cl_2. CH_2Cl_2 is known to react with the

reduced states of various metal complexes, and we believe that such a phenomenon is responsible for the irreversible nature of the second reduction step for some of the complexes in CH_2Cl_2.[20]

Reports on the substitution of one or more of the bpy ligands in $[Ru(bpy)_3]^{2+}$ with an additional chelating nitrogen donor ligand L are available in the literature. For instance, complexes of the type $[Ru(bpy)_2(Q)]^{2+}$ (Q = bpy with substituents displaying a negative inductive (−I) effect, or other π-accepting ligands) have been investigated with respect to their electrochemical and spectroscopic properties.[18] In those complexes, the oxidation as well as the first reduction step occurs at potentials different from those of $[Ru(bpy)_3]^{2+}$. Such ligands are usually better π-acceptors than bpy. Hence, those ligands are easier to reduce than bpy. Additionally, the lower lying π* orbitals of Q as compared to bpy allow for their better mixing with the Ru-based orbitals, thus influencing the metal based oxidation potentials as well. Energetically, the π* orbitals for the ligands L^1–L^6 are higher than bpy. Hence, they are more difficult to reduce than bpy, and this explains the absence of the third reduction process in **1**–**6** as compared to $[Ru(bpy)_3]^{2+}$. The same energetically higher π* orbitals avoid reasonable orbital mixing with the metal based d-orbitals and are responsible for the insulation of the oxidation potentials from the ligand substitution in **1**–**6**.

UV-vis-NIR spectroelectrochemistry and TD-DFT calculations

As expected from the electrochemical properties, the UV-vis signatures of the complexes **1**–**6** are very similar. For instance, 3^{2+} shows absorptions at 240, 255, and 284 nm, between 310 and 380 nm with a maximum at 360, and between 390 and 590 with maxima at 411 and 438 nm (Fig. 8, S2† and Table 6). For comparison, $[Ru(bpy)_3]^{2+}$ displays absorption bands at 243 and 286, in the range 310–360, and in the range 370–600 nm with a maximum at 450 (Table 6).[18] Structure based TD-DFT calculations were carried out to help in the assignment of the bands observed in the UV-vis-NIR spectra of the complexes. Calculations were performed on 3^{2+} and 6^{2+}, for which experimental structures are available and which can be used as representative examples respectively for the complexes with pyridyl-triazoles and bis-triazoles as ligands. Structural optimization with the functional BP86 produced good agreement between the bond lengths and bond angles of the experimental and calculated structures (Tables S2 and S3†). These calculations pointed out the presence of a predominantly ruthenium (about 75% contribution) centered HOMO, and bpy centered (about 70% contribution) LUMO for both 3^{2+} and 6^{2+} (Tables S4 and S5†). The bands at higher energies are either transitions based on the ligands or have mixed origin (Table 7). The transition at 284 is assigned to a d(Ru) → π*(tz) MLCT transition (Table 7 and Fig. 9). The high energy of this band is in keeping with the intuition that the triazole rings should contribute strongly to higher lying unoccupied orbitals. The bands between 310 and 360 nm are a mixture of d(Ru) → π*(tz) and d(Ru) → π*(bpy) MLCT transitions. Metal centered d → d transitions are likely to be hidden under these transitions.[18] TD-DFT confirms the low energy bands with maxima
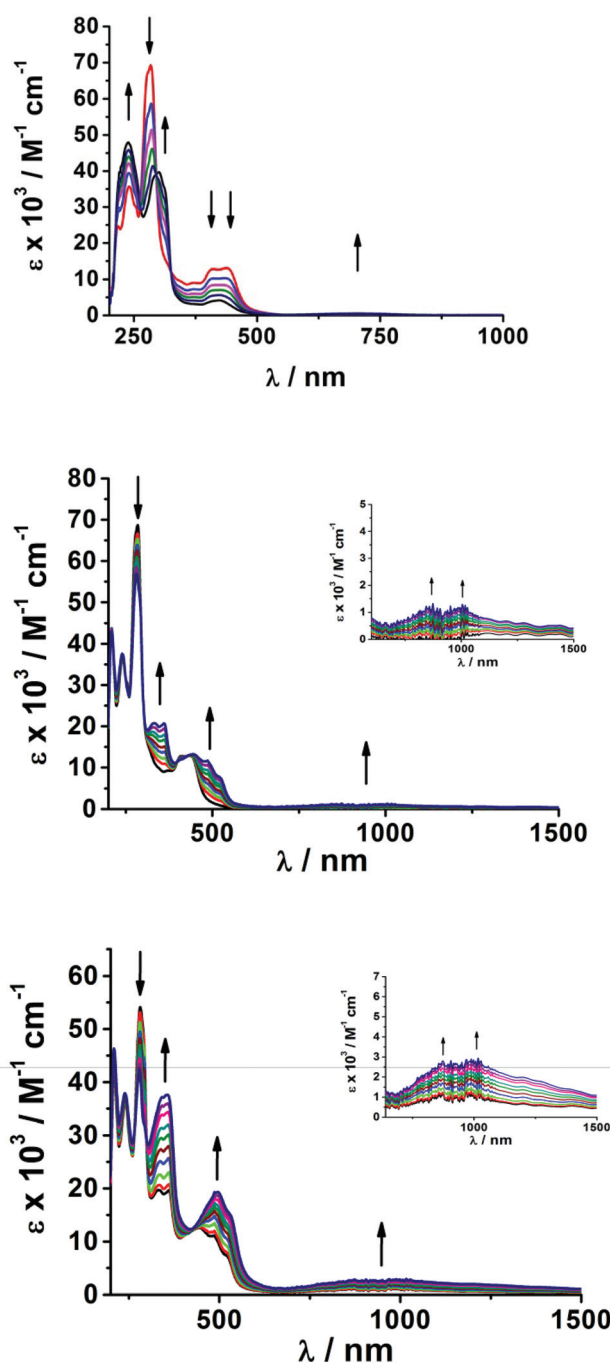
Fig. 8 Changes in the UV-vis-NIR spectrum of 3^{2+} during the first oxidation (top), the first reduction (middle) and the second reduction (bottom). The inset shows an expansion of the NIR region for the one-electron and two-electron reduced species.

at 411 and 438 nm as the d(Ru) → π*(bpy) ^{1}MLCT transition (Table 7 and Fig. 9). The one additional band observed for 3^{2+} (and also for 1^{2+} and 2^{2+}, Table 6) as compared to $[Ru(bpy)_3]^{2+}$ appears at 255 nm, and this band is assigned to a tz → bpy LLCT transition. This particular band is missing in the complexes 4^{2+}–6^{2+} which contain the bis-triazole ligands L^4–L^6. The origin of the transitions in 6^{2+} which contain a bis-triazole

Table 6 UV-vis-NIR data from spectroelectrochemistry[a]

$\lambda/nm\ (\varepsilon/M^{-1}\ cm^{-1})$

1^{2+}	242 (35 700), 254(32 700), 284 (77 300), 324 sh, 412 (12 300), 443 (12 600)
2^{2+}	241 (35 600), 254 (31 700), 285 (91 000), 324 sh, 413 (13 400), 444 (13 600)
3^{2+}	240 (35 600), 255 (sh), 284 (69 200), 360 sh, 411 (12 800), 438 (13 000)
4^{2+}	236 (70 500), 285 (91 200), 330 sh, 408 sh, 439 (15 300)
5^{2+}	242 (66 600), 285 (66 900), 330 sh, 402 sh, 439 (15 300)
6^{2+}	239 (66 200), 279 (63 700), 296 (67 800), 330 sh, 397 sh, 433 (30 800)
1^{3+}	244 (44 000), 255 sh, 286 (54 300), 314 sh, 414 (5200), 443 sh, 628 (830), 777 (700)
2^{3+}	241 (43 900), 255 sh, 289 (59 300), 314 sh, 413 (6100), 444 sh, 690 (1200), 930 (1120)
3^{3+}	238 (47 900), 250sh, 301 (39 700), 314 sh, 423 (4100), 438 sh, 680 (900), 700 (550)
4^{3+}	240 (47 000), 255sh, 305 (40 700), 320 sh, 425 (4200), 440 sh, 650 (1100), 700 (550)
5^{3+}	242 (34 200), 285 (38 500), 301 (37 300), 312 (34 900), 422 (4600), 577 (2200), 767 (1200)
6^{3+}	239 (66 700), 284 (35 000), 301 (37 300), 315 sh, 402 sh, 427 (15 200), 720 (1500)
$3^{+,b}$	210 (43 000), 240 (37 500), 255 sh, 282 (56 900), 333 (20 700), 361 (20 700), 406 sh, 444 (13 300), 486 (11 700), 520 sh, 873 (1300), 1004 (1300)
$5^{+,b}$	211 (61 200), 241 (80 800), 287 (75 900), 328 (32 800), 350 sh, 438 (15 500), 486 (12 100), 525 sh, 889 (1600), 988 (1500)
$6^{+,b}$	212 (134 600), 233 (142 500), 291 (137 400), 333 (59 700), 357 (58 800), 430 (31 200), 486 (28 200), 525 (sh), 869 (4000), 998 (4000)
3^{b}	209 (46 300), 239 (37 900), 279 (42 400), 295 sh, 343 (37 100), 356 (37 600), 496 (19 300), 530 sh, 873 (2800), 1017 (2900)
5^{b}	212 (65 200), 240 (72 000), 291 (50 100), 342 (51 900), 357 (52 300), 462 sh, 492 (21 300), 533 sh, 888 (3900), 988 (3700)
6^{b}	212 (148 200), 232 (146 300), 294 (103 400), 342 (103 200), 357 (104 900), 460 (sh), 497 (42 200), 532 (sh). 869 (7900) 998 (7900)

[a] From OTTLE spectroelectrochemistry in CH_2Cl_2–0.1 M Bu_4NPF_6 at 295 K. [b] Measurements were carried out in CH_3CN–0.1 M Bu_4NPF_6.

Table 7 Main TD-DFT calculated transitions of 3^{2+} compared with experimental data

Compound	Main contributing excitation (%)	Transition wavelength (nm)	Oscillator strength	Exp. transition wavelength (nm)	Molar absorption coefficient ($M^{-1}\ cm^{-1}$)
3^{2+}	HOMO−2 → LUMO (48)	426	0.135	438	13 000 M → L(bpy)
	HOMO−1 → LUMO+1 (23)				
	HOMO−1 → LUMO+1 (57)	406	0.085	411	12 800 M → L(bpy)
	HOMO → LUMO+7 (36)	332	0.078	360	sh M → L
	HOMO → LUMO+6 (23)				
	HOMO−2 → LUMO+5 (26)	322	0.061		
	HOMO−2 → LUMO+7 (21)				
	HOMO−2 → LUMO+6 (43)	316	0.077		
	HOMO−1 → LUMO+10 (63)	280	0.122	284	69 200 M → L(tz)
	Mixed[a]	272	0.230		
	Mixed[a]	266	0.444		
	Mixed[a]	262	0.248	255	sh
	HOMO−6 → LUMO+1 (33)	260	0.228	255	sh L → L

[a] Mixed refers to transitions where many different starting and target orbitals contribute to the transition.

ligand is similar to those in 3^{2+} (except for the band at 255 nm). The relevant frontier orbitals have been depicted in Fig. S3,† and the main transitions are tabulated in Table S6.† The molar extinction coefficient for the long wavelength band of 6^{2+} (Table 6) is approximately the double of those of the other complexes. This increase likely indicates better orbital overlap, leading to a larger transition probability for that transition in 6^{2+}. TD-DFT calculations delivered approximately the same oscillator strengths for all complexes. However, we would like to note that such calculations do not always provide good quantitative fits for molar extinction coefficients. Even though the electrochemical properties of the complexes **1–6** are virtually identical, small differences are observed in their UV-vis spectra.

To shed light on the electronic structures of the various redox forms of the complexes and to prove the reversibility of

the redox processes, UV-vis-NIR spectroelectrochemical measurements were carried out on the complexes. Spectroelectrochemical studies on the reduced complexes were carried out only on 3^{2+}, 5^{2+}, and 6^{2+} as representatives of the two classes of ligands used in this study. On scanning back the redox potentials to the starting potential after each redox step, the spectra of the original compounds were recovered in quantitative amounts. Hence these experiments provide proof for the reversibility of the redox processes. On one-electron oxidation, the MLCT bands for all complexes decrease in intensity (Fig. 8 and Table 6) as would be expected for electron removal from a metal centered orbital. Additionally, all one-electron oxidized species display weak absorption features in the red to the NIR region. These weak bands are reminiscent of the weak LMCT band(s) observed for $[Ru(bpy)_3]^{3+}$ (at 675 nm) and related species.[21] Hence we assign these weak absorption
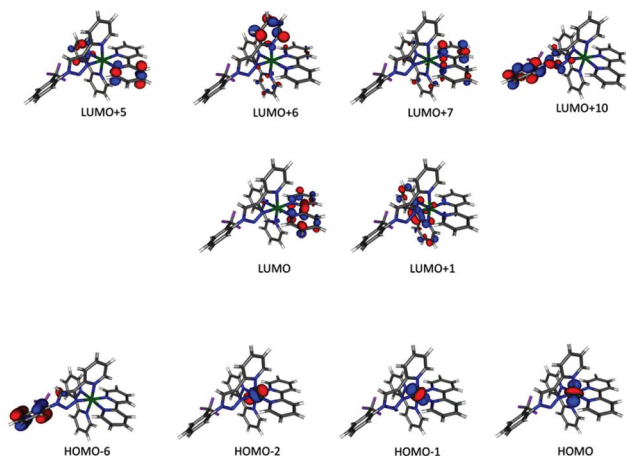
Fig. 9 Relevant calculated frontier orbitals (canonical orbitals) for the optical transitions observed in 3^{2+}. Orbitals are shown with an iso-value of 0.06.

bands to π (pyridyl-triazole) or π (bis-triazole) to partially filled dπ orbitals of the Ru(III) center. This assignment is supported by TD-DFT calculations on 3^{3+} and 6^{3+} which confirm the character of this transition as LMCT (Fig. 10, S4† and Table 8, S7†). Further transitions in the range of 400–450 nm are also all LMCT in character. Higher energy transitions are either intra-ligand or mixed in character (Fig. 10, S4† and Table 8, S7†). For 6^{3+}, certain higher energy transitions are also LMCT in nature.

The one-electron reduced complexes display various bands in the visible region that gain in intensity on reduction of the complexes with a further electron (Fig. 8, S2† and Table 6). These bands are assigned to MLCT transitions and are similar to those observed for $[Ru(bpy)_3]^+$.[22] TD-DFT calculations confirm the assignment of these bands as d(Ru) → π*(tz) and
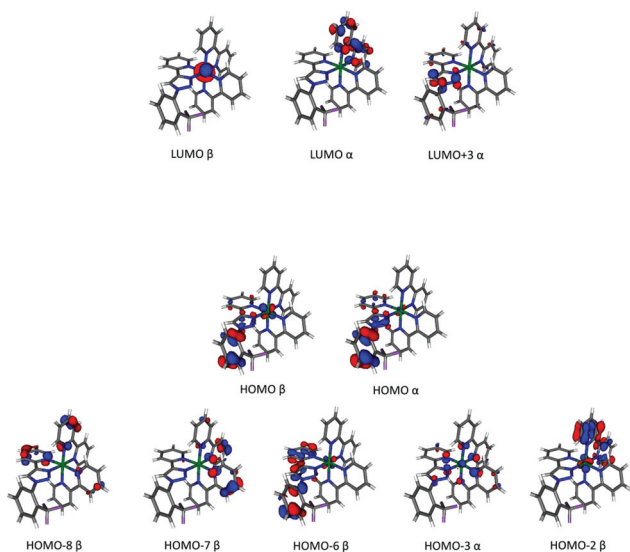
Fig. 10 Relevant calculated frontier orbitals (canonical orbitals) for the optical transitions observed in 3^{3+}. Orbitals are shown with an iso-value of 0.06.

d(Ru) → π*(bpy) MLCT transitions (Fig. 11, S5† and Table 9, S8†). Furthermore, a weak, broad structured band is observed in the NIR region on reducing the complexes with one-electron. This band gains in intensity on further reducing the complexes with a second electron. Such a band with vibronic coupling has previously been observed for $[Ru(bpy)_3]^+$. With the support of TD-DFT calculations we assign the broad features in the NIR region as a mixture of intra-ligand transitions within $(bpy)^{•-}$, inter-ligand charge transfer (ILCT), from $(bpy)^{•-}$ to L, and inter-valence charge transfer (IVCT) within the formulation $[Ru^{II}(bpy)^{•-}(bpy)L]^+$ (Fig. 11, S5 and Table 9, S8†). Further bands observed at higher energies are of intra-ligand and mixed nature. In keeping with the NIR bands observed for the two-electron reduced complexes, these species can be formulated as $[Ru^{II}(bpy)^{•-}_2L]^+$. Changes in the UV-vis-NIR spectrum of 3^{2+} during oxidation and reduction have been plotted in wavenumbers in Fig. S6.†

EPR spectroscopy and DFT calculations

Both the one-electron oxidized and the one-electron reduced forms of the complexes were investigated using EPR spectroscopy to determine the site of electron transfer in these complexes and to unravel possible similarities and differences in the EPR characteristics of these paramagnetic species. The one-electron oxidized forms 1^{3+}–3^{3+} of the complexes with the pyridyl-triazole ligands are EPR-silent in fluid solutions at 295 K. At 110 K these complexes display a signal with axial symmetry with g-values for instance of $g_\parallel$ = 2.74 and $g_\perp$ = 2.06 (Fig. 12 and Table 10). $[Ru(bpy)_3]^{3+}$ also displays an anisotropic spectrum with an axial symmetry.[23] However, in that case, $g_\parallel <$ $g_\perp$, and the g-anisotropy is larger (Table 10). In contrast to 1^{3+}–3^{3+}, the complexes 4^{3+}–6^{3+} containing the bis-triazole ligands are EPR silent down to 110 K. Thus, it is seen that the substitution of a bpy ligand in $[Ru(bpy)_3]^{3+}$ with either L^1–L^3 ligands containing pyridyl-triazole donors, or L^4–L^6 containing the bis-triazole donors have a significant influence on their EPR properties. The symmetry of the electronic ground state of the complexes 1^{3+}–3^{3+} is inverted as compared to $[Ru(bpy)_3]^{3+}$ as seen from the inversion of the $g_\parallel$ and $g_\perp$ values. For 4^{3+}–6^{3+}, the inclusion of the symmetric bis-triazoles L^4–L^6 seems to speed up the spin–lattice relaxation process, possibly through the influence of close-lying states, thus leading to enormous line broadening and EPR silence at 110 K. The EPR signatures, or the absence of it in some cases, clearly point to species with predominantly metal centered spin in all the cases. DFT calculations also predict a larger number of closely spaced states for 6^{3+} as compared to 3^{3+}. Thus, the energy differences between the orbital containing the unpaired electron and the next three orbitals are 0.01, 0.06 and 0.11 eV for 6^{3+}, and the corresponding values for 3^{3+} are 0.06, 0.18 and 0.23 eV respectively. The differences obtained from DFT calculations fit with the experimentally observed faster relaxation for 6^{3+} as compared to 3^{3+}.

The one-electron reduced forms 1^{1+}–6^{1+} were also probed by EPR spectroscopy. All the complexes display strong signals in fluid solutions at 295 K. The g-value in all cases is very close to

Table 8 Main TD-DFT calculated transitions of 3^{3+} compared with experimental data

Compound	Main contributing excitation (%)	Transition wavelength (nm)	Oscillator strength	Exp. transition wavelength (nm)	Molar absorption coefficient (M^{-1} cm^{-1})
3^{3+}	HOMO−6(β) → LUMO(β) (73)	757	0.008	700	550 L(tz) → M
	HOMO(β) → LUMO(β) (26)	724	0.007		L(tz)/M → M
	HOMO−2(β) → LUMO(β) (35)				
	HOMO−7(β) → LUMO(β) (74)	429	0.019	438	sh L(bpy) → M
	HOMO−8(β) → LUMO(β) (68)	424	0.014	423	4100 L → M
	HOMO−7(β) → LUMO(β) (21)				
	HOMO−3(α) → LUMO(α) (49)	337	0.23	314	sh L/M → L
	Mixed[a]	299	0.058	301	39 700
	Mixed[a]	288	0.108		
	Mixed[a]	286	0.068		
	Mixed[a]	285	0.078		
	Mixed[a]	267	0.070	238	47 900
	Mixed[a]	266	0.060		
	Mixed[a]	265	0.066		
	HOMO(α) → LUMO+3(α) (30)	264	0.100		IL

[a] Mixed refers to transitions where many different starting and target orbitals contribute to the transition.
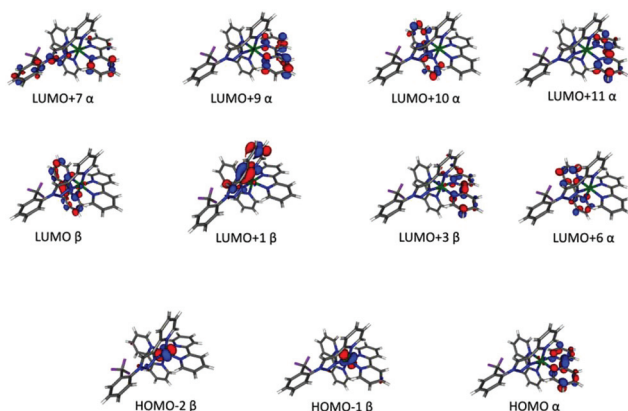
Fig. 11 Relevant calculated frontier orbitals (canonical orbitals) for the optical transitions observed in 3^+. Orbitals are shown with an iso-value of 0.06.

that this signal does not arise from organic impurities. The EPR data obtained for 1^+–6^+ match well with those of $[Ru(bpy)_3]^+$.[24] The appearance of an EPR signal in fluid solution at 295 K is a clear indication of a ligand centered spin. In addition, comparison of the EPR, electrochemical and UV-vis data to those of the parent tris-bpy-Ru(II) complex clearly establishes the reduction as being bpy centered.

In order to verify the conclusions drawn from the EPR measurements, DFT calculations were carried out on selected complexes. Geometry optimizations were performed using the BP86 functional. A look at the spin densities by using the Löwdin population analysis for 3^{3+} and 6^{3+} shows more than 90% spin density to be located at the ruthenium center (Fig. 13, S8†). The absolute g-anisotropy is accurately reproduced by the DFT calculations (Δg of 0.7 from both experiment and calculations). This result thus strongly corroborates the large g-anisotropy observed for 1^{3+}–3^{3+} and the "EPR-silence" of 4^{3+}–6^{3+} species at 110 K and confirms the formulation $[Ru^{+III}(bpy)_2(L)]^{3+}$ for these one-electron oxidized complexes.

In contrast to the one-electron oxidized complexes, for the one-electron reduced forms 3^+ and 6^+ more than 90% spin density is found to be located at the bpy ligand(s). A similar situation has been observed for $[Ru(bpy)_3]^+$, where the spin density is entirely located on a bpy ligand. The question of

2.0 (Fig. 12, S7† and Table 11), and the peak-to-peak separation is between 40 and 50 G. In the case of 3^+, the hyperfine coupling to the nitrogen atoms was partially resolved. However, an appropriate simulation was not possible because of the lack of a highly resolved spectrum (Fig. 12). Control experiments with UV-vis-NIR spectroscopy were used to verify

Table 9 Main TD-DFT calculated transitions of 3^+ compared with experimental data

	Main contributing excitation (%)	Transition wavelength (nm)	Oscillator strength	Exp. transition wavelength (nm)	Molar absorption coefficient (M^{-1} cm^{-1})
3^+	HOMO(α) → LUMO+6(α) (41)	1088	0.003	1004	1300 L → L
	HOMO(α) → LUMO+7(α) (23)				
	HOMO(α) → LUMO+6(α) (45)	1014	0.002		
	HOMO(α) → LUMO+7(α) (22)				
	HOMO(α) → LUMO+9(α) (72)	840	0.015	873	1300 IL
	HOMO(α) → LUMO+10(α) (92)	529	0.018	520	sh L → L
	HOMO−2(β) → LUMO(β) (40)	471	0.077	486	11 700 M → L(bpy)
	HOMO−2(β) → LUMO+1(β) (22)				
	HOMO(α) → LUMO+11(α) (66)	444	0.064	444	13 300 IL
	HOMO−1(β) → LUMO+3(β) (51)	394	0.058	406	sh M → L(bpy)
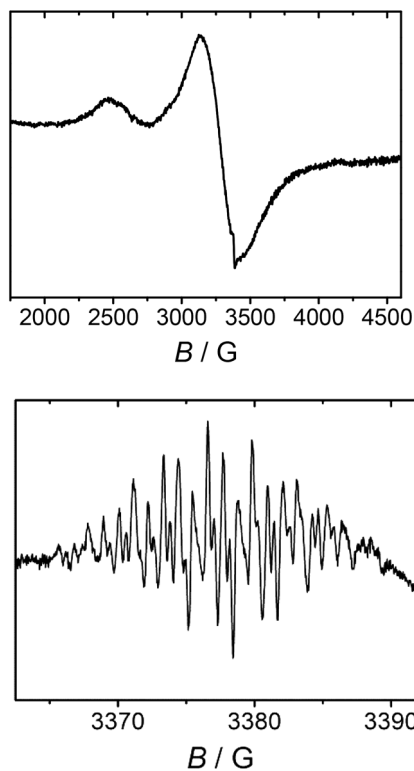
Fig. 12 EPR spectra of *in situ* electrochemically generated $\mathbf{1^{3+}}$ at 110 K (top) and $\mathbf{3^{+}}$ at 295 K.

Table 10 EPR data for the one-electron oxidized complexes[a]

	$g_{\parallel}$	$g_{\perp}$	g_{av}	Δg
$\mathbf{1^{3+}}$	2.74	2.06	2.29	0.68
$\mathbf{2^{3+}}$	2.74	2.06	2.29	0.68
$\mathbf{3^{3+}}$	2.75	2.07	2.29	0.68
$\mathbf{4^{3+}}$	n.o.	n.o.	n.o.	n.o.
$\mathbf{5^{3+}}$	n.o.	n.o.	n.o.	n.o.
$\mathbf{6^{3+}}$	n.o.	n.o.	n.o.	n.o.
$[\mathrm{Ru(bpy)}_3]^{3+,b}$	1.14	2.64	2.14	1.50

[a] From measurements in $\mathrm{CH_3CN}$–0.1 M $\mathrm{Bu_4NPF_6}$ at 295 K. [b] From ref. 23. n.o. = no EPR signal was observed down until 110 K.

Table 11 EPR data for the one-electron reduced complexes[a]

	g_{iso}
$\mathbf{1^{+}}$	1.995
$\mathbf{2^{+}}$	1.996
$\mathbf{3^{+}}$	2.004
$\mathbf{4^{+}}$	1.997
$\mathbf{5^{+}}$	1.997
$\mathbf{6^{+}}$	1.997
$[\mathrm{Ru(bpy)}_3]^{+,b}$	1.998

[a] From measurements in $\mathrm{CH_3CN}$–0.1 M $\mathrm{Bu_4NPF_6}$ at 295 K. [b] From ref. 24.

localisation *versus* delocalisation of the spin density on the bpy ligands has been extensively investigated for $[\mathrm{Ru(bpy)}_3]^{+}$, and the consensus is for a localized case with the spin density
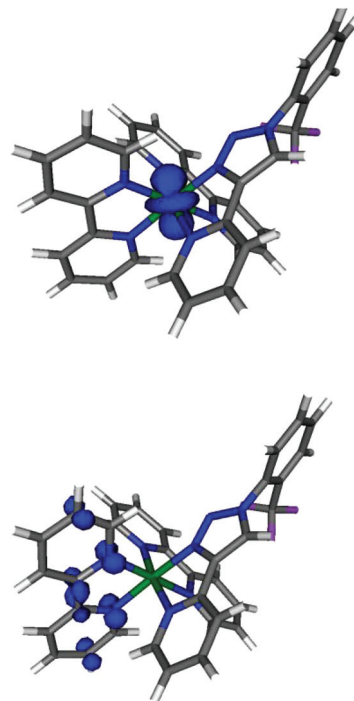
Fig. 13 Spin density plot for $\mathbf{3^{3+}}$ (top) and $\mathbf{3^{+}}$ (bottom). Spin densities are shown with an iso-value of 0.01.

localized in one bpy ring.[18,22–24] For the present case, DFT calculations deliver a localized situation for $\mathbf{3^{+}}$ and a delocalized picture for $\mathbf{6^{+}}$. However, we would like to note that DFT methods are known to exaggerate delocalization, and hence in the present case the reduced complex is likely best formulated as $[\mathrm{Ru(bpy)}^{\bullet-}(\mathrm{bpy})\mathrm{L}]^{+}$, with the spin density being localized at one bpy ligand. The UV-vis and the EPR data also corroborate this formulation. However, the possibility of electron hopping between the two bpy rings cannot be ruled out.

Conclusions

Summarizing, six Ru(II) complexes have been presented here with pyridyl-triazole and bis-triazole ligands. Structural analysis reveals shorter Ru–N(triazole) bonds as compared to the Ru–N(bpy) bonds in complexes with mixed pyridyl-triazole donors. Comparison with the complexes containing bis-triazoles and the parent complex $[\mathrm{Ru(bpy)}_3]^{2+}$ clearly shows the attenuated π-accepting capacity of pyridyl-triazole and bis-triazoles as compared to bpy. All complexes display one reversible oxidation and two reversible reduction steps, the potentials of which are unperturbed by ligand substitution. In comparison to $[\mathrm{Ru(bpy)}_3]^{2+}$, a third reduction is not observed for the present complexes in $\mathrm{CH_3CN}$ proving the higher reduction potentials for the pyridyl-triazole and bis-triazole ligands as compared to bpy. The reduction steps of the complexes are sensitive to solvent effects as seen from the comparison between electrochemical measurements in $\mathrm{CH_3CN}$ and $\mathrm{CH_2Cl_2}$. Despite the invariant electrochemical responses,

subtle changes as a function of ligand substitution are observed in the UV-vis-NIR and EPR spectra of the complexes in the various investigated redox states. Thus, in UV-vis-NIR spectra of the oxidized form, the position of the LMCT band is seen to vary with the change in the ligand. The reduced forms of the complexes display structured absorptions in the NIR region. The oxidized forms of the complexes display different characteristics depending on the nature of the chelating ligand. The complexes $[Ru(bpy)_2(L)]^{3+}$ with the pyridyl-triazole ligands show an inverse axial symmetry in their EPR spectrum as compared to $[Ru(bpy)_3]^{3+}$; the complexes containing bis-tri-azole ligands are "EPR silent" till 110 K. The one-electron reduced forms of all the complexes display bpy-centered spin and can be best formulated as $[Ru(bpy)^{\bullet-}(bpy)(L)]^+$. DFT calculations of the spin density distribution for the one-electron oxidized and the one-electron reduced states confirm the spin to be located on the ruthenium center for the oxidized complex, and on bpy for the reduced complex. This contribution is one of the rare occasions where a combined structural, electrochemical, UV-vis-NIR and EPR spectroelectrochemical approach, as well as DFT studies, has been used to elucidate the electronic structures of metal complexes containing "click" derived triazole ligands. Our studies show that the electronic structures of metal complexes can be influenced by substituting a bpy ligand in $[Ru(bpy)_3]^{n+}$ with pyridyl-triazoles or bis-triazoles. The electrochemical responses however remain similar to $[Ru(bpy)_3]^{n+}$.

Experimental section

Materials and physical methods

$Ru(bpy)_2Cl_2$ was purchased from ABCR. All the reagents were used as supplied. The solvents used for metal complex synthesis were dried and distilled under argon and degassed by common techniques prior to use.

The ^{1}H NMR spectra were recorded on a Bruker AC 250 or a Jeol ECS 400 spectrometer. Mass spectrometry was performed on a Bruker Daltronics Mictrotof-Q mass spectrometer. Electronic absorption studies were performed using on J&M TIDAS, Avantes spectrometer system and Shimadzu UV 3101 PC spectrophotometers. Spectroelectrochemistry was performed using an optically transparent thin-layer electrode (OTTLE) cell.[25] Spectra were recorded by continuously scanning the potentials as shown in the cyclic voltammograms by using the diode-array spectrometer. Reversibility of the redox waves was tested by scanning back the potential to the starting value. On doing this, the original spectra of the complexes were generated back quantitatively, demonstrating the reversibility of the redox waves. EPR spectra in the X-band were recorded with a Bruker System EMX. Bulk-electrolysis was performed for generating the oxidized and reduced species for EPR measurements. Approximately 10^{-5} mmol solutions were used. For the low temperature measurements, the samples were electrolyzed at room temperature, and immediately frozen with liquid nitrogen in an EPR sample holder. Cyclic

voltammetry was carried out in 0.1 M Bu_4NPF_6 solutions using a three-electrode configuration (a glassy-carbon working electrode, a Pt counter electrode, and the Ag/AgCl reference) and a PAR 273 potentiostat and function generator or a Versastat 4 potentiostat. The ferrocene/ferrocenium (Fc/Fc^+) couple served as an internal reference. Elemental analyses were performed using the Perkin-Elmer Analyzer 240 or an ELEMENTAR Vario EL III instrument.

Synthesis of ligands

Ligands L^1,[9a] L^2,[11b] L^3,[9b] L^4,[16] and L^5,[3c] have previously been reported in the literature.

In this particular work ligands L^1 and L^2 were synthesized following a new click procedure described by Hohloch et al.[12a]

2-Pyridyl-acetylene (1 eq., 3 mmol) and the corresponding azide (1 eq., 3 mmol) were mixed in a small vial and copper(I)-iodide (0.01 eq., 0.03 mmol, 6 mg), potassium *tert*-butoxide (0.02 eq., 0.06 mmol, 6 mg) and 3-methyl-1-(2-(methylthio)-phenyl)-4-phenyl-1,2,3-triazolium iodide (0.01 eq., 0.03 mmol, 0.011 g) were added. After a short time the mixture evolved heat and solidified. The crude products were purified by flash silica gel column chromatography using dichloromethane first, followed by dichloromethane–methanol 9 : 1, giving the responding ligands as off-white powders in good yields of 90%.

2-(1-(4-Isopropylphenyl)-1*H*-1,2,3-triazol-4-yl)pyridine (L^1)

^{1}H NMR (250 MHz, CDCl$_3$; 25 °C, TMS): δ (ppm) = 1.26 (d, J = 7 Hz, 6H); 2.97 (hept, J = 7 Hz, 1H); 7.22–7.24 (m, 1H); 7.25–7.28 (m, 2H); 7.67–7.70 (m, 2H); 7.76–7.79 (m, 1H); 8.20–8.24 (m, 1H); 8.54 (s, 1H) 8.57–8.60 (m, 1H); ^{13}C NMR (60 MHz, CDCl$_3$, 25 °C, TMS): δ (ppm) = 23.8; 33.8; 119.9; 120.4; 127.7; 149.9 MS (ESI): found m/z 264.1381. calcd m/z 264.1375 [C$_{16}$H$_{16}$N$_4$]; elemental analysis calcd (%) for [C$_{16}$H$_{16}$N$_4$] C 72.70, H 6.10, N 21.20; found C 72.16, H 6.19, N 20.76.

2-(1-(4-Butoxyphenyl)-1*H*-1,2,3-triazol-4-yl)pyridine (L^2)

^{1}H NMR (250 MHz, CDCl$_3$; 25 °C, TMS): δ (ppm) = 0.94 (t, J = 6.5 Hz, 3H); 1.49 (sex, J = 6.5 Hz, 2H); 1.79 (pent, J = 6.5 Hz, 2H); 4.00 (t, J = 6.5 Hz, 2H); 6.97–7.02 (m, 2H); 7.20–7.25 (m, 1H); 7.62–7.70 (m, 2H); 7.76–7.80 (m, 1H); 8.22 (d, J = 8 Hz, 1H), 8.48 (s, 1H); 8.59 (d, J = 4.25 Hz, 1H); ^{13}C NMR (60 MHz, CDCl$_3$, 25 °C, TMS): δ (ppm) = 13.7; 19.1; 31.1; 68.1; 115.3; 120.1; 120.4; 122.0; 122.9; 130.2; 136.9; 148.7; 149.4; 150.1; 159.5 MS (ESI): found m/z 294.1483 calcd m/z 294.1481 [C$_{17}$H$_{18}$N$_4$O]; elemental analysis calcd (%) for [C$_{17}$H$_{18}$N$_4$O] C 69.37, H 6.16, N 19.03; found C 68.66, H 6.20, N 18.29.

The ligand L^6 was synthesized using a standard procedure reported by Fletcher et al.

Copper sulfate pentahydrate (0.4 eq., 1.2 mmol, 300 mg), sodium ascorbate (0.8 eq., 2.4 mmol, 480 mg) and potassium carbonate (2 eq., 6 mmol, 830 mg) were mixed in a flask. Afterwards 30 ml of *tert*-butanol was added, followed by the 2-(tri-fluoromethyl)-phenylazide (2 eq., 6 mmol, 1.13 g) and 1,4-bis-(trimethylsilyl)-1,3-butadiyne (1 eq., 3 mmol, 0.582 g). To the

mixture were added 30 ml of water and 3 ml of pyridine. The mixture was capped and stirred at room temperature for up to 3 days. After the reaction, the mixture was diluted with dichloromethane (150 ml) and extracted with 5% ammonia solution in water 5 times (each washing 50 ml). The organic layers were separated and dried over sodium sulfate (40 g) and the solvents were evaporated under reduced pressure. The crude products were purified by silica flash column chromatography using dichloromethane as an eluent giving the desired product as a brownish powder in good yields up to 85%.

1,1′-Bis(2-(trifluoromethyl)phenyl)-1H,1′H-4,4′-bi(1,2,3-triazole) (L^6)

^{1}H NMR (250 MHz, CDCl$_3$; 25 °C, TMS): δ (ppm) = 7.56–7.63 (m, 2H); 7.67–7.81 (m, 4H); 7.87–7.93 (m, 2H); 8.40 (s, 2H) ^{13}C NMR (100 MHz, CDCl$_3$, 25 °C, TMS): δ (ppm) = 121.3; 123.7; 124.0; 126.4; 126.6; 126.7; 127.1; 127.4; 127.5; 127.6; 127.7; 129.1; 130.8; 133.2; 134.7; 139.8; ^{19}F NMR (376 MHz, CDCl$_3$, 25 °C): δ (ppm) = −59.0 MS (ESI): found m/z 447.0773 calcd m/z 447.0769 [C$_{18}$H$_{10}$N$_6$F$_6$ + Na]; elemental analysis calcd (%) for [C$_{18}$H$_{10}$N$_6$F$_6$] C 50.95, H 2.38, N 19.81; found C 50.91, H 2.41, N 19.12.

Synthesis of the ruthenium(II)-complexes

All complexes were synthesized following the general procedure:

Ru(bpy)$_2$Cl$_2$ (1 eq., 0.2 mmol, 96 mg) and silver perchlorate (2 eq., 0.4 mmol, 86 mg) were refluxed in 10 ml ethanol under an argon atmosphere for 2 h. Afterwards the mixture was filtered into a solution of the corresponding ligand in 10 ml ethanol. The reaction was then heated under reflux overnight. The solvent was then evaporated until only 2 ml ethanol was left. Sodium perchlorate (8 eq., 1.6 mmol, 225 mg) was added. After 5 minutes of heavy stirring, the mixture was diluted with 100 ml water and the orange solids were filtered and dried at room temperature. The crude product was then purified by alumina column chromatography using dichloromethane–methanol 99 : 1. All volatilities were removed and the orange product was once again precipitated from 5 ml acetone using a saturated sodium perchlorate–water (100 ml) solution and filtered. The orange powder was air dried overnight to yield the desired product in excellent yields.

[Ru(bpy)$_2$(L^1)](ClO$_4$)$_2$ (1(ClO$_4$)$_2$). Yield: 85% (1.7 mmol, 149 mg); ^{1}H NMR (250 MHz, acetone-d$_6$; 25 °C, TMS): δ (ppm) = 1.23 (d, J = 7 Hz, 6H); 2.99 (hept, J = 6.75 Hz, 1H); 7.44–7.71 (m, 9H); 7.75 (d, J = 5 Hz, 1H); 8.07 (d, J = 5.5 Hz, 1H); 8.14–8.26 (m, 7H); 8.34 (d, J = 5 Hz, 1H); 8.47 (d, J = 8 Hz, 1H); 8.86–8.74 (m, 4H); 9.78 (s, 1H) MS (ESI): found m/z 339.0916 calcd m/z 339.0891 [C$_{36}$H$_{32}$N$_8$Ru^{2+}]; elemental analysis calcd (%) for [C$_{36}$H$_{32}$N$_8$RuCl$_2$O$_8$ + 1.5CH$_2$Cl$_2$] C 44.86, H 3.51, N 11.16; found C 44.75, H 2.99, N 12.10.

[Ru(bpy)$_2$(L^2)](ClO$_4$)$_2$ (2(ClO$_4$)$_2$). Yield: 82% (1.65 mmol, 148 mg); ^{1}H NMR (250 MHz, acetone-d$_6$; 25 °C, TMS): δ (ppm) = 0.94 (t, J = 6.5 Hz, 3H); 1.46 (d, J = 6.5 Hz, 2H); 1.75 (pent, J = 6.5 Hz, 2H); 4.05 (t, J = 6.5 Hz, 2H); 7.07 (d, J = 9 Hz, 2H); 7.43–7.62 (m, 5H); 7.68 (d, J = 8.75 Hz, 2H); 7.91 (d, J = 5.25

Hz, 1H); 8.02 (d, J = 5.0 Hz, 1H); 8.11–8.23 (m, 6H); 8.29 (d, J = 5.5 Hz, 1H); 8.46 (d, J = 8 Hz, 1H); 8.70–8.83 (m, 4H); 9.70 (s, 1H) MS (ESI): found m/z 354.0949 calcd m/z 354.0944 [C$_{37}$H$_{34}$N$_8$Ru^{2+}]; elemental analysis calcd (%) for [C$_{37}$H$_{34}$N$_8$RuCl$_2$O$_8$] C 49.01, H 3.78, N 12.36; found C 48.84, H 4.13, N 11.92.

[Ru(bpy)$_2$(L^3)](ClO$_4$)$_2$ (3(ClO$_4$)$_2$). Yield: 77% (1.5 mmol, 135 mg); ^{1}H NMR (250 MHz, acetone-d$_6$, 25 °C, TMS): δ (ppm) = 7.42–7.52 (m, 2H); 7.58–7.66 (m, 3H); 7.86–8.00 (m, 5H); 8.06–8.29 (m, 7H); 8.36 (d, J = 6.25 Hz, 1H); 8.71 (d, J = 8 Hz, 1H); 8.77–8.88 (m, 3H); 9.55 (s, 1H) ^{19}F NMR (235 MHz, acetone-d$_6$, 25 °C): δ (ppm) = −60.1; MS (ESI): found m/z 352.0584 calcd m/z 352.0594 [C$_{34}$H$_{25}$N$_8$F$_3$Ru^{2+}]; elemental analysis calcd (%) for [C$_{34}$H$_{25}$N$_8$F$_3$RuCl$_2$O$_8$] C 45.24, H 2.79, N 12.41; found C 44.98, H 2.82, N 12.18.

[Ru(bpy)$_2$(L^4)](ClO$_4$)$_2$ (4(ClO$_4$)$_2$). Yield: 75% (0.15 mmol; 160 mg); ^{1}H NMR (400 MHz, acetone-d$_6$; 25 °C, TMS): δ (ppm) = 0.60 (d, J = 6.8 Hz, 6H); 0.91 (d, J = 6.8 Hz, 6H); 1.08 (d, J = 6.8 Hz, 6H); 1.24 (d, J = 6.8 Hz, 6H); 1.51 (hept, J = 6.8 Hz, 2H); 2.61 (hept, J = 6.4 Hz, 2H); 7.26–7.32 (m, 2H); 7.36–7.42 (m, 2H); 7.44–7.50 (m, 2H); 7.51–7.58 (m, 2H); 7.71–7.78 (m, 2H); 8.04–8.13 (m, 2H); 8.21–8.27 (m, 2H); 8.29–8.35 (m, 4H); 8.70–8.76 (m, 2H); 8.82–8.88 (m, 2H); 9.16 (s, 2H) MS (ESI): found m/z 435.1717 calcd m/z 435.1705 [C$_{48}$H$_{52}$N$_{10}$Ru^{2+}]; elemental analysis calcd (%) for [C$_{48}$H$_{52}$N$_{10}$RuCl$_2$O$_8$] C 53.93, H 4.90, N 13.10; found C 54.40, H 5.20, N 12.85.

[Ru(bpy)$_2$(L^5)](ClO$_4$)$_2$ (5(ClO$_4$)$_2$). Yield: 74% (0.148 mmol; 133 mg); ^{1}H NMR (250 MHz, acetone-d$_6$; 25 °C, TMS): δ (ppm) = 7.50–7.61 (m, 10H); 7.72–7.77 (m, 4H); 8.15–8.22 (m, 6H); 8.42–8.46 (m, 2H); 8.75–8.80 (m, 4H); 9.47 (s, 2H) MS (ESI): found m/z 351.0762 calcd m/z 351.0766 [C$_{36}$H$_{28}$N$_{10}$Ru^{2+}]; elemental analysis calcd (%) for [C$_{36}$H$_{28}$N$_{10}$RuCl$_2$O$_8$] C 48.01, H 3.13, N 15.55; found C 48.52, H 3.39, N 15.85.

[Ru(bpy)$_2$(L^6)](ClO$_4$)$_2$ (6(ClO$_4$)$_2$). Yield: 86% (0.172 mmol; 178 mg); ^{1}H NMR (250 MHz, acetone-d$_6$; 25 °C, TMS): δ (ppm) = 7.46–7.51 (m, 2H); 7.63–7.69 (m, 2H); 7.85–7.98 (m, 8H); 8.09–8.14 (m, 2H); 8.18–8.22 (m, 2H); 8.24–8.30 (m, 2H); 8.40–.43 (m, 2H); 8.72–8.76 (m, 2H); 8.79–8.83 (m, 2H); 9.25 (s, 2H); ^{19}F NMR (376 MHz, acetone-d$_6$, 25 °C): δ (ppm) = −60.0; MS (ESI): found m/z 937.0757 calcd m/z 937.0770 [C$_{38}$H$_{26}$N$_{10}$F$_6$RuCl$_1$O$_4^+$]; elemental analysis calcd (%) for [C$_{38}$H$_{26}$N$_{10}$F$_6$RuCl$_2$O$_8$] C 44.03, H 2.53, N 13.51; found C 43.78, H 2.59, N 13.09.

X-ray crystallography

X-ray quality crystals of L^3 and L^4 were obtained by slow evaporation of a concentrated diethylether solution at room temperature. A severely disordered diethyl ether molecule was found in L^3. X-ray quality crystals of 3(ClO$_4$)$_2$, 4(ClO$_4$)$_2$ and 6(ClO$_4$)$_2$ were obtained by slow diffusion of n-hexane into a concentrated solution of these complexes in dichloromethane at 8 °C. Single crystal X-ray structural studies were performed on a Bruker Kappa Apex II duo or a Bruker smart AXS diffractometer. Data were collected at 100(2) K using graphite-monochromated Mo Kα radiation (λ_α = 0.71073 Å). The strategy for the data collection was evaluated by using the CrysAlisPro CCD

or Smart software. The data were collected by the standard 'phi-omega scan techniques, and were scaled and reduced using CrysAlisPro RED software or Saint+ software. The structures were solved by direct methods using SHELXS-97 and refined by full matrix least-squares with SHELXL-97,[26] refining on F^2. CCDC 846891, 846892, 892295, and 906187 contain the supplementary crystallographic files for this work.

DFT calculations

DFT calculations were done with the ORCA 2.9.1 program[27] package using the BP86 and B3LYP functionals for the geometry optimization and single-point calculations respectively.[28] The restricted and unrestricted DFT method was employed for closed and open shell molecules respectively. All calculations were run with empirical van der Waals correction.[29] Convergence criteria were set to default for the geometry-optimizations (OPT) and tight for SCF calculations (TIGHTSCF). Relativistic effects were included with the zeroth-order relativistic approximation (ZORA).[30] Triple-ζ-valence basis sets (TZVPP-ZORA)[31] were employed for all atoms. Calculations were performed using the resolution of the identity approximation[32] with matching auxiliary basis sets. Low-lying excitation energies were calculated with time-dependent DFT (TD-DFT). Solvent effects were taken into account with the conductor-like screening model (COSMO)[33] for all calculations. Spin densities were calculated according to the Löwdin population analysis.[34] The contribution of molecular fragments to molecular orbitals was analyzed using the MOAnalyzer tool.[35] Molecular orbitals and spin densities were visualized using the Molekel 5.4.0.8 program.[36]

Acknowledgements

References

1 (a) V. Rostovtsev, L. G. Green, V. V. Fokin and K. B. Sharpless, *Angew. Chem., Int. Ed.*, 2002, **41**, 2596; (b) C. V. Tornoe, C. Christensen and M. Meldal, *J. Org. Chem.*, 2002, **67**, 3057.

2 (a) L. Liang and D. Astruc, *Coord. Chem. Rev.*, 2011, **255**, 2933; (b) H. Struthers, T. L. Mindt and R. Schibli, *Dalton Trans.*, 2010, **39**, 675; (c) J. D. Crowley and D. McMorran, in *Topic in Heterocyclic Chemistry*, ed. J. Kosmrlj, Springer, Berlin/Heidelberg, 2012, vol. 28, pp. 31; (d) D. Schweinfurth, N. Deibel, F. Weisser and B. Sarkar, *Nachr. Chem.*, 2011, **59**, 937; (e) G. Aromi, L. A. Barrios, O. Robeau and P. Gamez, *Coord. Chem. Rev.*, 2011, **255**, 485.

3 (a) Y. Li, J. C. Huffman and A. H. Flood, *Chem. Commun.*, 2007, 2692; (b) R. M. Meudtner, M. Ostermeier, R. Goddard, C. Limberg and S. Hecht, *Chem.–Eur. J.*, 2007, **13**, 9834; (c) J. T. Fletcher, B. J. Bumgarner, N. D. Engels and D. A. Skoglund, *Organometallics*, 2008, **27**, 5430; (d) W. W. Yang, L. Wang, Y. W. Zhong and Y. Yao, *Organometallics*, 2011, **30**, 2236; (e) C. Richardson, C. M. Fitchett, F. R. Keene and P. J. Steel, *Dalton Trans.*, 2008, 2534; (f) B. Schulze, C. Friebe, M. D. Hager, A. Winter, R. Hoogenboom, H. Goerls and U. S. Schubert, *Dalton Trans.*, 2009, 787; (g) B. Happ, C. Friebe, A. Winter, M. D. Hager, R. Hoogenboom and U. S. Schubert, *Chem.–Asian. J.*, 2009, **4**, 154; (h) C. E. Welby, S. Grkinic, A. Zahid, B. S. Uppal, E. A. Gibson, C. R. Rice and P. I. P. Elliot, *Dalton Trans.*, 2012, **41**, 7637; (i) J. G. Vos, J. G. Haasnnot and G. Vos, *Inorg. Chim. Acta*, 1983, **71**, 155; (j) R. Hage, R. Prins, J. G. Haasnoot, J. Reedijk and J. G. Vos, *J. Chem. Soc., Dalton Trans.*, 1987, 1389.

4 (a) K. N. Swanick, S. Ladouceur, E. Zysman-Colman and Z. Ding, *Chem. Commun.*, 2012, **48**, 3179; (b) G. F. Manbeck, W. W. Brennessel and R. Eisenberg, *Inorg. Chem.*, 2011, **50**, 3431; (c) M. Mydlak, C. Bizzarri, D. Hartmann, W. Sarfert, G. Schmid and L. De Cola, *Adv. Funct. Mater.*, 2010, **20**, 1812; (d) L. Donato, P. Abel and E. Zysman-Colman, *Dalton Trans.*, 2013, **42**, 8402; (e) A. Baron, C. Herrero, A. Quaranta, M.-F. Charlot, W. Leibl, B. Vauzeilles and A. Aukauloo, *Inorg. Chem.*, 2012, **51**, 5985; (f) A. Mattiuzzi, I. Jabin, C. Moucheron and A. K. De-Mesmaeker, *Dalton Trans.*, 2011, **40**, 7395.

5 (a) J. D. Crowley and P. H. Bandeen, *Dalton Trans.*, 2010, **39**, 612; (b) S.-Q. Bai, S. Leelasubcharoen, X. Chen, L. L. Koh, J.-L. Juo and T. S. A. Hor, *Cryst. Growth Des.*, 2010, **10**, 1715; (c) V. Steinmetz, F. Couty and O. R. P. David, *Chem. Commun.*, 2009, 343; (d) B. Collason, N. L. Paul, Y. L. Mest and O. Reinaud, *J. Am. Chem. Soc.*, 2010, **132**, 4393; (e) D. Urankar, A. Pevec and J. Kosmrlj, *Cryst. Growth Des.*, 2010, **10**, 4920; (f) A. H. Younes, R. J. Clark and L. Zhu, *Supramol. Chem.*, 2012, **24**, 696; (g) K. A. Stevenson, C. F. C. Melan, O. Fleischel, R. Wang and A. Petitjean, *Cryst. Growth Des.*, 2012, **12**, 5169; (h) N. G. White and P. D. Beer, *Supramol. Chem.*, 2012, **24**, 473.

6 (a) M. Ostermeier, M.-A. Berlin, R. A. Meudtner, S. Demeshko, F. Meyer, C. Limberg and S. Hecht, *Chem.–Eur. J.*, 2010, **16**, 10202; (b) P. M. Guha, H. Phan, J. S. Kinyon, W. S. Brotherton, K. Sreenath, J. T. Simmons, Z. Wang, R. J. Clark, N. S. Dalal, M. Shatruk and L. Zhu, *Inorg. Chem.*, 2012, **51**, 3465.

7 (a) S. Gu, H. Xu, N. Zhang and Y. Chen, *Chem.–Asian. J.*, 2010, **5**, 1677; (b) X. C. Cambeiro and M. A. Pericas, *Adv. Synth. Catal.*, 2011, **353**, 113; (c) R. Lalrempuia, N. D. McDaniel, H. Müller-Bunz, S. Bernhard and M. Albrecht, *Angew. Chem., Int. Ed.*, 2010, **49**, 9765; (d) K. J. Kilpin, U. S. D. Paul, A.-L. Lee and J. D. Crowley, *Chem. Commun.*, 2011, **47**, 328; (e) R. Saravanakumar, V. Ramkumar and S. Sankararaman, *Organometallics*, 2011, **30**, 1689; (f) C. Hua, K. Q. Vuong, M. Bhadbhade and

B. A. Messerle, *Organometallics*, 2012, **31**, 1790; (*g*) S. Hohloch, L. Suntrup and B. Sarkar, *Organometallics*, 2013, DOI: 10.1021/om4009185.

8 (*a*) A. Maisonial, P. Serafin, M. Traikia, E. Debiton, V. Théry, D. J. Aitken, P. Lemoine, B. Viossat and A. Gautier, *Eur. J. Inorg. Chem.*, 2008, 298; (*b*) A. Chevry, M. L. Teyssot, A. Maisonial, P. Lemoine, B. Viossat, M. Traikia, D. J. Aitken, G. Alves, L. Morel, L. Nauton and A. Gautier, *Eur. J. Inorg. Chem.*, 2010, 3513.

9 (*a*) D. Schweinfurth, R. Pattacini, S. Strobel and B. Sarkar, *Dalton Trans.*, 2009, 9291; (*b*) D. Schweinfurth, S. Strobel and B. Sarkar, *Inorg. Chim. Acta*, 2011, **374**, 253.

10 (*a*) D. Schweinfurth, F. Weisser, D. Bubrin, L. Bogani and B. Sarkar, *Inorg. Chem.*, 2011, **50**, 6114; (*b*) D. Schweinfurth, J. Klein, S. Hohloch, S. Dechert, S. Demeshko, F. Meyer and B. Sarkar, *Dalton Trans.*, 2013, **42**, 6944; (*c*) D. Schweinfurth, J. Kryzstek, I. Schapiro, S. Demeshko, J. Klein, J. Telser, A. Ozarowski, C.-Y. Su, F. Meyer, M. Atanasov, F. Neese and B. Sarkar, *Inorg. Chem.*, 2013, **52**, 6880.

11 (*a*) D. Schweinfurth, S. Demeshko, M. M. Khusniyarov, S. Dechert, V. Gurram, M. R. Buchmeiser, F. Meyer and B. Sarkar, *Inorg. Chem.*, 2012, **51**, 7592; (*b*) D. Schweinfurth, C.-Y. Su, S.-C. Wei, P. Braunstein and B. Sarkar, *Dalton Trans.*, 2012, **41**, 12984.

12 (*a*) S. Hohloch, C.-Y. Su and B. Sarkar, *Eur. J. Inorg. Chem.*, 2011, 3067; (*b*) S. Hohloch, B. Sarkar, L. Nauton, F. Cisnetti and A. Gautier, *Tetrahedron Lett.*, 2013, **54**, 1808; (*c*) S. Hohloch, D. Scheiffele and B. Sarkar, *Eur. J. Inorg. Chem.*, 2013, 3956.

13 S. Hohloch, W. Frey, C.-Y. Su and B. Sarkar, *Dalton Trans.*, 2013, **42**, 11355.

14 (*a*) G. K. Lahiri and W. Kaim, *Angew. Chem., Int. Ed.*, 2007, **46**, 1778; (*b*) J. R. Gispert, *Coordination Chemistry*, Wiley-VCH, Weinheim, 2008; (*c*) J. Boyer, J. Rochford, M.-K. Tsai, J. T. Muckerman and E. Fujita, *Coord. Chem. Rev.*, 2010, **254**, 309; (*d*) D. E. Polyansky, J. T. Muckerman, J. Rochford, R. Zong, R. P. Thummel and E. Fujita, *J. Am. Chem. Soc.*, 2011, **133**, 14649; (*e*) G. K. Lahiri and W. Kaim, *Dalton Trans.*, 2010, **39**, 4471.

15 (*a*) M. G. Sommer, D. Schweinfurth, F. Weisser, S. Hohloch and B. Sarkar, *Organometallics*, 2013, **32**, 2069; (*b*) N. Deibel, D. Schweinfurth, J. Fiedler, S. Zalis and B. Sarkar, *Dalton Trans.*, 2011, **40**, 9925; (*c*) N. Deibel, D. Schweinfurth, S. Hohloch, J. Fiedler and B. Sarkar, *Chem. Commun.*, 2012, **48**, 2388.

16 G. Guisado-Barrios, J. Bouffard, B. Donnadieu and G. Bertrand, *Organometallics*, 2011, **30**, 6017.

17 M. Obata, A. Kitamura, A. Mori, C. Kameyama, J. A. Czaplewska, R. Tanaka, I. Kinoshita, T. Kusumoto, H. Hashimoto, M. Harada, Y. Mikata, T. Funabiki and S. Yano, *Dalton Trans.*, 2008, 3292.

18 A. Juris, V. Balzani, F. Barigelletti, S. Campagna, P. Belser and A. von Zelewsky, *Coord. Chem. Rev.*, 1988, **84**, 85–277.

19 N. G. Connelly and W. E. Geiger, *Chem. Rev.*, 1996, **96**, 877.

20 R. Pattacini, S. Jie and P. Braunstein, *Chem. Commun.*, 2009, 890.

21 M. K. Nazeeruddin, S. M. Zakeeruddin and K. Kalyanasundaram, *J. Phys. Chem.*, 1993, **97**, 9607.

22 (*a*) C. M. Elliott, *J. Chem. Soc., Chem. Commun.*, 1980, 261; (*b*) G. A. Heath and L. Y. Yellowlees, *J. Chem. Soc., Chem. Comm.*, 1981, 287; (*c*) G. A. Heath and L. Y. Yellowlees, *Chem. Phys. Lett.*, 1982, **92**, 646.

23 R. E. DeSimone and R. S. Drago, *J. Am. Chem. Soc.*, 1970, **92**, 2343.

24 D. E. Morris, K. W. Hanck and M. K. DeArmond, *J. Am. Chem. Soc.*, 1983, **105**, 3032.

25 M. Krejcik, M. Danek and F. Hartl, *J. Electroanal. Chem.*, 1991, **317**, 179.

26 G. M. Sheldrick, *SHELXL-97, Program for refinement of crystal structures*, University of Göttingen, Göttingen, Germany, 1997.

27 F. Neese, *WIREs Comput. Mol. Sci.*, 2012, **2**, 73.

28 (*a*) A. D. Becke, *J. Chem. Phys.*, 1993, **98**, 5648; (*b*) A. D. Becke, *Phys. Rev. A*, 1988, **38**, 3098; (*c*) C. Lee, W. Yang and R. G. Parr, *Phys. Rev. B: Condens. Matter*, 1988, **37**, 785.

29 S. Grimme, J. Antony, S. Ehrlich and H. Krieg, *J. Chem. Phys.*, 2010, **132**, 154104.

30 C. van Wüllen, *J. Chem. Phys.*, 1998, **109**, 392.

31 D. A. Pantazis, X.-Y. Chen, C. R. Landis and F. Neese, *J. Chem. Theory Comput.*, 2008, **4**, 908.

32 (*a*) F. Neese, *J. Comput. Chem.*, 2003, **24**, 1740; (*b*) F. Neese, F. Wennmohs, A. Hansen and U. Becker, *Chem. Phys.*, 2009, **356**, 98; (*c*) O. Vahtras, J. Almlöf and M. W. Feyereisen, *Chem. Phys. Lett.*, 1993, **213**, 514; (*d*) J. L. Whitten, *J. Chem. Phys.*, 1973, **58**, 4496.

33 (*a*) A. Klamt and G. Schüürmann, *J. Chem. Soc., Perkin Trans. 2*, 1993, 799; (*b*) S. Sinnecker, A. Rajendran, A. Klamt, M. Diedenhofen and F. Neese, *J. Phys. Chem. A*, 2006, **110**, 2235.

34 P.-O. Löwdin, *J. Chem. Phys.*, 1950, **18**, 365.

35 M. U. Delgado-Jaime and S. DeBeer, *J. Comput. Chem.*, 2012, **33**, 2180.

36 S. Portmann, *Molekel, version 5.4.0.8*, CSCS/UNI, Geneva, Switzerland, 2009.